



Article

Study of the Electrochemical Behavior of N-Substituted-4-Piperidones Curcumin Analogs: A Combined Experimental and Theoretical Approach

John Amalraj ¹, Claudia E. Vergara ², Matías Monroy-Cárdenas ^{1,3}, Ramiro Araya-Maturana ^{1,3,*} 
and Maximiliano Martínez-Cifuentes ^{4,*} 

¹ Instituto de Química de Recursos Naturales, Universidad de Talca, Talca 3460000, Chile

² Departamento de Ciencias Básicas, Facultad de Ciencias, Universidad Santo Tomás, Avda. Carlos Schorr 255, Talca 8370003, Chile

³ MIBI: Interdisciplinary Group on Mitochondrial Targeting and Bioenergetics, Universidad de Talca, P.O. Box 747, Talca 3460000, Chile

⁴ Departamento de Química Orgánica, Facultad de Ciencias Químicas, Universidad de Concepción, Edmundo Larenas 129, Concepción 4070371, Chile

* Correspondence: raraya@utalca.cl (R.A.-M.); maxmartinez@udec.cl (M.M.-C.)

Abstract: The electrochemical behavior of N-methyl- and N-benzyl-4-piperidone curcumin analogs were studied experimentally and theoretically. The studied compounds present different substituents at the *para* position in the phenyl rings (-H, -Br, -Cl, -CF₃, and -OCH₃). We assessed their electrochemical behavior by differential pulse and cyclic voltammetry, while we employed density functional theory (DFT) M06 and M06-2x functionals along with 6-311+G(d,p) basis set calculations to study them theoretically. The results showed that compounds suffer a two-electron irreversible oxidation in the range of 0.72 to 0.86 V, with surface concentrations ranging from 1.72×10^{-7} to 5.01×10^{-7} mol/cm². The results also suggested that the process is diffusion-controlled for all compounds. M06 DFT calculations showed a better performance than M06-2x to obtain oxidation potentials. We found a good correlation between the experimental and theoretical oxidation potential for N-benzyl-4-piperidones ($R^2 = 0.9846$), while the correlation was poor for N-methyl-4-piperidones ($R^2 = 0.3786$), suggesting that the latter suffer a more complex oxidation process. Calculations of the BDEs for labile C-H bonds in the compounds suggested that neither of the two series of compounds has a different tendency for a proton-coupled electron transfer (PCET) oxidation process. It is proposed that irreversible behavior is due to possible dimerization of the compounds by Shono-type oxidation.

Keywords: curcumin; electrochemistry; DFT; curcuminoids; piperidones; benzyl derivatives



Citation: Amalraj, J.; Vergara, C.E.; Monroy-Cárdenas, M.; Araya-Maturana, R.; Martínez-Cifuentes, M. Study of the Electrochemical Behavior of N-Substituted-4-Piperidones Curcumin Analogs: A Combined Experimental and Theoretical Approach. *Int. J. Mol. Sci.* **2022**, *23*, 15043. <https://doi.org/10.3390/ijms232315043>

Academic Editor: Mihai V. Putz

Received: 23 October 2022

Accepted: 25 November 2022

Published: 30 November 2022

Publisher's Note: MDPI stays neutral with regard to jurisdictional claims in published maps and institutional affiliations.



Copyright: © 2022 by the authors. Licensee MDPI, Basel, Switzerland. This article is an open access article distributed under the terms and conditions of the Creative Commons Attribution (CC BY) license (<https://creativecommons.org/licenses/by/4.0/>).

1. Introduction

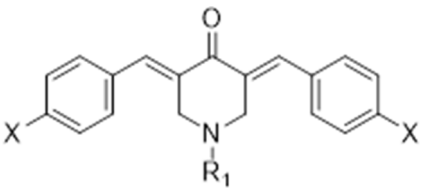
Curcumin (diferuloylmethane), a yellow compound isolated from the turmeric plant (*Curcuma longa*), is one of the most extensively studied naturally occurring polyphenols. The pharmacological properties of curcumin, related to a large variety of diseases, have attracted great interest [1–7]. Despite these interesting pharmacological properties, it suffers from several drawbacks for practical applications, due to its poor bioavailability, which is a consequence of low chemical stability and low water solubility [8–10]. The latter has prompted the search for curcumin analogs that keep or improve their bioactivity, while, at the same time, overcoming their drawbacks. Several structural modifications have been afforded to enhance the bioavailability of curcumin [11–13]. It has been proposed that compounds possessing a β -diketone moiety, as in the case of curcumin, are a substrate of liver aldo-keto reductases, which probably contribute to their rapid in vivo metabolism [12,14,15]. To avoid this drawback, multiple synthetic alternatives have been assayed, among which replacing the β -diketone moiety with a heterocyclic ring has shown

to be effective [12,16]. Among the alternatives, synthetic analogs of curcumin possessing a 4-piperidone scaffold have shown high bioactivity, e.g., as anti-inflammatory and anticancer agents [17–21].

One of the aspects of curcumin that have presented some controversy is its electrochemical behavior [22–25]. During recent years, the electrochemical behavior of some of the derived curcuminoid families also have been studied, e.g., the electrochemistry of pyrazole derivatives of curcumin [26], the electrochemistry and antioxidant capacity of curcumin derivatives obtained by esterification of its phenol groups [27], and the electronic and conductance properties of a couple of thiophene curcuminoids using electrochemical techniques, ultraviolet spectroscopy, and DFT calculations [27]. However, until now, the electrochemical behavior of N-substituted-4-piperidone curcumin analogs has not been reported, which seems relevant to study due to their interesting pharmacological properties, which have been suggested to be associated with the electron transfer process [13]. Besides our previous work on the reactivity of these compounds, only theoretical work dealing with the potential technological application for the non-linear optics of this type of curcuminoid can be found [16,28].

Based on the above, in this work we propose to study the electrochemical behavior of N-substituted-4-piperidone curcuminoid analogs (Table 1). The effect of different substituents on the aromatic rings and the variation in the N-substituent of the piperidone ring (methyl and benzyl) could help in the understanding of the electrochemical behavior and help in the design of curcumin piperidone derivatives with biological activity, besides determining the oxidation potentials that could be useful in obtaining derivatives by electrochemical synthesis [29–31]. We employ differential pulse and cyclic voltammetry to experimentally study the electrochemistry of compounds, and DFT calculations to obtain theoretical redox potentials, which are then compared with those obtained experimentally, assessing the effects of the substituents at the phenyl substituent.

Table 1. Studied compounds.



Compound	R ₁	X
C1	CH ₃	H
C2	CH ₃	Br
C3	CH ₃	Cl
C4	CH ₃	CF ₃
C5	CH ₃	OCH ₃
C6	CH ₂ Ph	H
C7	CH ₂ Ph	Br
C8	CH ₂ Ph	Cl
C9	CH ₂ Ph	CF ₃
C10	CH ₂ Ph	OCH ₃

2. Results and Discussion

2.1. Synthesis

Compounds were obtained by the base-catalyzed aldolic condensation of N-methyl or N-benzyl-4-piperidones with the corresponding aldehyde (Table 2). Moderate to high yields were achieved, ranging from 48% for compound C9 to 88% for compound C5. Compounds C1 to C8 and C10 have been previously described (see references indicated in Table 2), while compound C9 is described here for the first time.

Table 2. Synthesis of the obtained compounds.

Compound	% Yield	Ref.
C1	71	[1,3]
C2	62	[2]
C3	71	[1,3]
C4	72	[4]
C5	88	[1,3,4]
C6	81	[5]
C7	81	[5]
C8	50	[5]
C9	48	This work
C10	58	[5]

2.2. Differential Pulse Voltammetry (DPV) Results

DPV results reveal that derivatives exhibited one well-defined anodic peak at potentials higher than +0.7 V versus Ag/AgCl (non-aqueous) (Figure 1 and Table 3). Oxidation peak potential values for the derivatives with electron-withdrawing groups were shifted towards more positive values, whereas derivatives with electron-releasing groups were shifted towards negative values. Similarly, when we compare the oxidation peak potential of N-methyl-substituted derivatives (C1 to C5) with N-benzyl-substituted derivatives (C6 to C10), the latter shifted the oxidation potential towards more positive values.

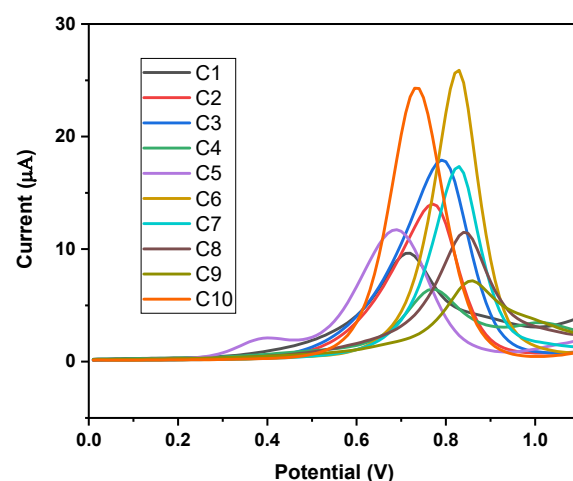


Figure 1. DP voltammograms of 2.0 mM solutions of compounds. Non-aqueous medium: 0.1 M of TBAP in CH₃CN.

2.3. Number of Electrons (n) Calculation

Our results showed that by increasing the scan rate, the peak potential is shifted to more positive potentials. Laviron's equation was used to estimate n as follows [32]:

$$E_p = E^0 + (RT/\alpha nF)[\ln(RTk_s/\alpha nF) - \ln v], \quad (1)$$

where E is the potential; E⁰ is the formal standard potential; k_s is the standard heterogeneous reaction rate constant; n is the transfer electron number; α refers to the charge-transfer coefficient; v is scan rate; R is the gas constant; T is the temperature; and F is the Faraday constant. When plotting the graph between E_p versus ln v, the slope gives the value of

$RT/\alpha nF$ ($\alpha = 0.5$); from this, we can calculate the number of electrons involved in the process (Table 4). In this way, n was found to be 2, implying that two electrons were transferred in the electrochemical redox reaction.

Table 3. Oxidation potentials of the compounds.

Compound	Eox (V)
C1	0.720
C2	0.770
C3	0.790
C4	0.770
C5	0.690
C6	0.830
C7	0.830
C8	0.840
C9	0.860
C10	0.730

Table 4. Number of electrons transferred (n) and surface concentration (Γ) for all the compounds.

Compound	n	Γ (mol/cm ²)
C1	1.93	2.67×10^{-7}
C2	1.77	3.55×10^{-7}
C3	1.88	4.65×10^{-7}
C4	2.19	1.72×10^{-7}
C5	1.69	2.43×10^{-7}
C6	1.68	5.01×10^{-7}
C7	1.80	3.69×10^{-7}
C8	1.78	2.76×10^{-7}
C9	2.10	2.07×10^{-7}
C10	1.87	4.89×10^{-7}

2.4. Surface Concentration

The surface concentrations of piperidone derivatives (Γ) were calculated employing the following equation:

$$I = n^2 F^2 A \Gamma \nu / 4RT, \quad (2)$$

where I is the peak current; $n = 2$ (number of electrons involved in the electrochemical process); F is the Faraday constant $96,485 \text{ C mol}^{-1}$; A is the surface area, 0.0707 cm^2 (the diameter of the working electrode, the glassy carbon electrode, is 0.3 cm , and from this, the surface area of the electrode was calculated); ν represents the scan rate; R is the gas constant, $8.314 \text{ JK}^{-1} \text{ mol}^{-1}$; and $T = 293 \text{ K}$. If we plot the graph of I_p versus the scan rate, which conforms to the following equation: $I_p (\mu\text{A}) = 0.721\nu + 10.223$ ($R^2 = 0.9153$), in this equation the slope, gives the value of $n^2 F^2 A \Gamma / 4RT$, from which we can calculate Γ . The results are presented in Table 4.

In the electrochemical process, there is an important difference between the concentration of a species at the surface of the electrode and its concentration at some distance from it, generally known as bulk concentration. The surface concentration depends on the rate at which the reactants are brought to the electrode surface by either diffusion or flow processes, which determines the rate of the electrochemical reaction.

All compounds exhibit a surface concentration in the order of 10^{-7} mol/cm^2 , compound C4 (N-methyl-4-piperidone with trifluoromethyl in phenyl rings) has the lowest value (1.72×10^{-7}), and compound C6 (N-benzyl-4-piperidone unsubstituted in phenyl rings) has the highest value (5.01×10^{-7}).

2.5. Cyclic Voltammetry Characterization

Scan rate has a great influence on the redox process of the electrode surface. Therefore, cyclic voltammograms of 2 mM of the derivatives were recorded in the scan rate range from 10 to 500 mVs^{-1} and the peak current increased with increased scan rate for all compounds (Figures 2a and 3a). The linear relationships of the square root of the scan rate and the scan rate on the peak current are shown in Figures 2c and 3c.

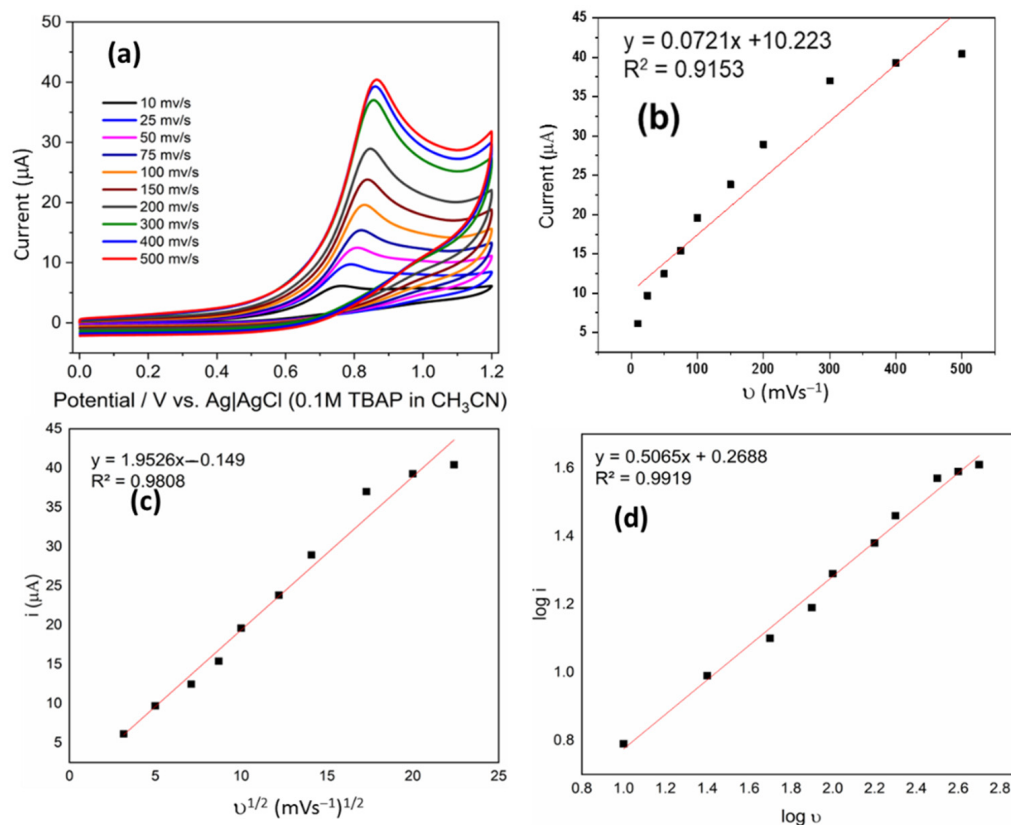


Figure 2. (a) Cyclic voltammograms of 2 mM of C1 in 0.1 M solution of TBAP in CH_3CN at different scan rates. (b) Linear relationship between i and ν . (c) Linear relationship between i and $\nu^{1/2}$ (d) Linear relationship between $\log i$ and $\log \nu$.

The dependence between I_p and ν shows a good linear correlation; the relationship can be presented by the following equation: $I_p (\mu\text{A}) = 0.0721\nu (\text{V/s}) + 10.223$ ($R^2 = 0.9153$) (Figure 2b). However, I_p on $\nu^{1/2}$ has better linear correlation, whose relationship can be presented by the following equation: $I_p (\mu\text{A}) = 1.9526 (\text{V}^{1/2}/\text{s}^{1/2}) - 0.149$ ($R^2 = 0.9808$) (Figure 2c). A similar analysis was performed for the compound 7, which shows $I_p (\mu\text{A}) = 0.1354\nu (\text{V/s}) + 21.558$ ($R^2 = 0.9597$) (Figure 3b), and for i_p on $\nu^{1/2}$, $I_p (\mu\text{A}) = 3.6023 (\text{V}^{1/2}/\text{s}^{1/2}) + 2.8508$ ($R^2 = 0.9926$) (Figure 3c). These observations strongly suggest that redox reactions of both derivatives are diffusion-controlled. Similar analyses were performed for all derivatives, and similar behavior was found in all cases.

Figures 2d and 3d shows the relationship between the logarithm of redox peak current and the logarithm of scan rate, which conformed to the following equation: $\log I_p (\text{A}) = 0.5065 \text{Log } \nu (\text{V/s}) + 0.2688$ ($R^2 = 0.9919$). As is known, the slope close to 0.5 is ascribed to a diffusion-controlled process, whereas the slope close to 1.0 is ascribed to an adsorption-controlled process.

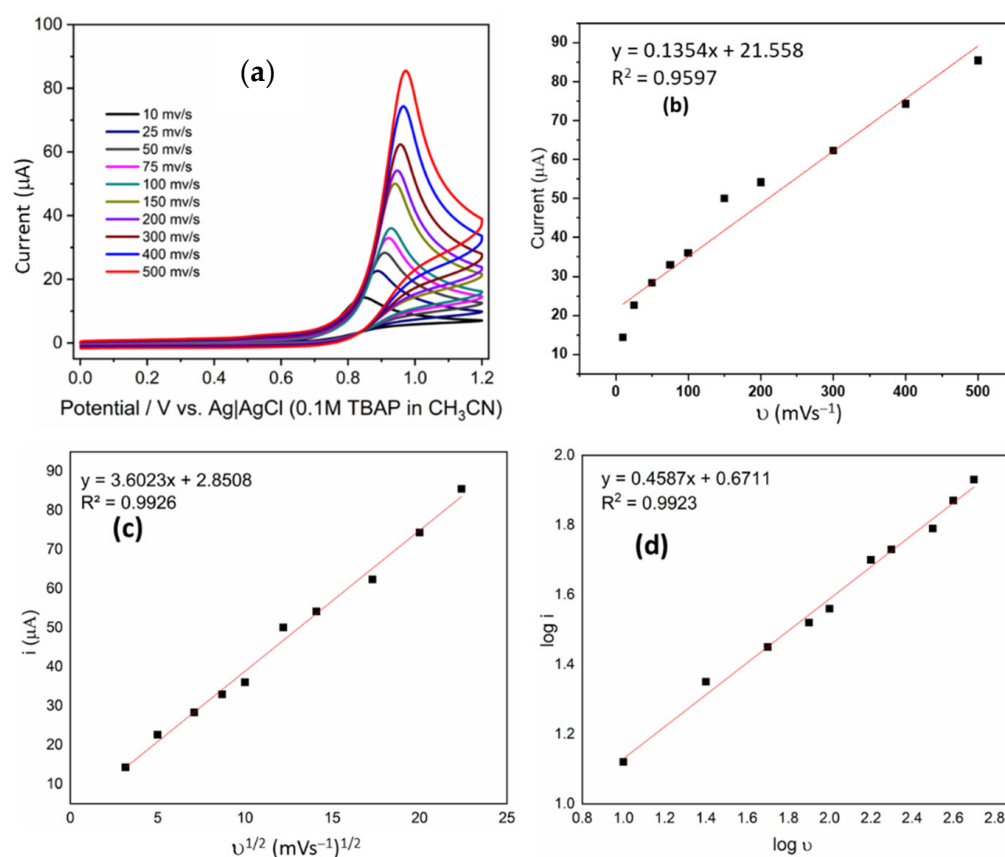


Figure 3. (a) Cyclic voltammograms of 2 mM of C6 in 0.1 M solution of TBAP in CH₃CN at different scan rates. (b) Linear relationship between i and v . (c) Linear relationship between i and $v^{1/2}$ (d) Linear relationship between $\log i$ and $\log v$.

2.6. Quantum Chemical Calculation

The oxidation potentials at DFT M06 and M06-2x level using 6-311+G(d,p) basis set were obtained for the ten derivatives. M06-2X functionals have been extensively used to calculate redox potentials [33–37]; however, in the specific case of oxidation potential, previous work has shown that functionals with high levels of Hartree–Fock (HF) exchange percentage tend to significantly overestimate the potential [38]. Therefore, we tested M06-2X (54% HF) and M06 functionals to obtain the potentials. The number of electrons transferred in the reactions, according to Laviron’s equation in Section 3.2, was two. Accordingly, we considered the two possible electronic states for oxidized species (singlet and triplet dications) for the calculations. Tables 5 and 6 show the values for experimental and theoretical oxidation potentials calculated with M06-2X and M06 functionals, respectively. In all cases, the mean absolute error (MAE) for M06 was lower than for M06-2X, which agrees with what has been previously reported [38]. MAE values are still overestimated with the M06 functional, but they are in the range of previous work of calculated oxidation potentials [39]. Based on the above, we use data obtained with the M06 functional to discuss the results.

Taking both series (N-methyl and N-benzyl) together, experimental and theoretical potentials did not correlate well, neither when considering the oxidized species as a triplet, nor as a singlet ($R^2 = 0.0796$ for singlet, $R^2 = 0.1667$ for triplet). However, when both series were treated separately, it was found that the series with the N-benzyl group at the piperidone ring presented a good correlation between experimental and theoretical oxidation potential.

Figure 4 presents the correlation between experimental and theoretical oxidation potential for the N-methyl (A) and N-benzyl (B) series considering the oxidized species

as a singlet, and for the N-methyl (C) and N-benzyl (D) series considering the oxidized species as a triplet.

Table 5. Experimental and theoretical oxidation potential (M06-2X) for all compounds, considering the oxidized species in the singlet state.

N-Substituent	Compound	Eox [V]			Exp	Error [V] (S)	Error [V] (T)
		M06-2X (S)	M06-2X (T)				
N-methyl	C1	2.26	1.96	0.72	1.54	1.24	
	C2	2.07	2.02	0.77	1.3	1.25	
	C3	2.05	1.98	0.79	1.26	1.19	
	C4	2.44	2.32	0.77	1.67	1.55	
	C5	1.60	1.45	0.69	0.91	0.76	
				MAE	1.34	1.20	
N-benzyl	C6	1.99	1.92	0.83	1.16	1.09	
	C7	2.05	1.98	0.83	1.22	1.15	
	C8	2.05	2.00	0.84	1.21	1.16	
	C9	2.29	2.25	0.86	1.43	1.39	
	C10	1.55	1.43	0.73	0.82	0.7	
				MAE	1.17	1.10	

Table 6. Experimental and theoretical oxidation potential (M06) for all compounds, considering the oxidized species in the singlet state.

N-Substituent	Compound	Eox [V]			Exp	Error [V] (S)	Error [V] (T)
		M06 (S)	M06 (T)				
N-methyl	C1	1.85	1.69	0.72	1.13	0.97	
	C2	1.75	1.66	0.77	0.98	0.89	
	C3	1.74	1.70	0.79	0.95	0.91	
	C4	2.07	1.99	0.77	1.33	1.22	
	C5	1.37	1.33	0.69	0.68	0.64	
				MAE	1.01	0.93	
N-benzyl	C6	1.57	1.58	0.83	0.74	0.75	
	C7	1.62	1.58	0.83	0.79	0.75	
	C8	1.67	1.55	0.84	0.83	0.71	
	C9	1.76	1.82	0.86	0.90	0.96	
	C10	1.21	1.23	0.73	0.48	0.50	
				MAE	0.75	0.73	

For the series with N-benzyl (compounds C6 to C10), good correlations were found considering both kinds of oxidized species, triplet or singlet ($R^2 = 0.8886$ and $R^2 = 0.9846$, respectively). Meanwhile, the series with the N-methyl group did not show a good correlation between experimental and theoretical oxidation potentials, neither when considering the oxidized species as triplet nor as singlet ($R^2 = 0.4918$ and $R^2 = 0.3786$, respectively).

Considering that the N-benzyl derivative series presented a good correlation between experimental and theoretical oxidation potentials, unlike that evidenced for the N-methyl series, it can be suggested that oxidation of this last series of compounds did not occur by a simple mechanism. The above indicates that variation of the substituent at nitrogen is a key factor that determines the redox behavior of these derivatives. In addition, based on the structural analysis mentioned above, it is reasonable to consider that the trend for both series will remain independent of the addition of more compounds for each series.

Triplet oxidized species for all compounds present a similar geometry, regardless of the substituent on the N-position or phenyl rings. However, for singlet oxidized species, the behavior varies between the N-methyl and N-benzyl series (Figure 5). For the N-methyl series, the oxidized species of compounds C2, C3, and C5 (with p-Br, p-Cl, and p-OCH3 in

the phenyl rings) present a notable geometry distortion of the piperidone ring, which does not occur for **C1** and **C4** (unsubstituted and with p-CF₃ in the phenyl rings). On the other hand, all oxidized species of the N-benzyl series present a notable geometrical distortion of the piperidone ring, regardless of the substituent on the phenyl rings.

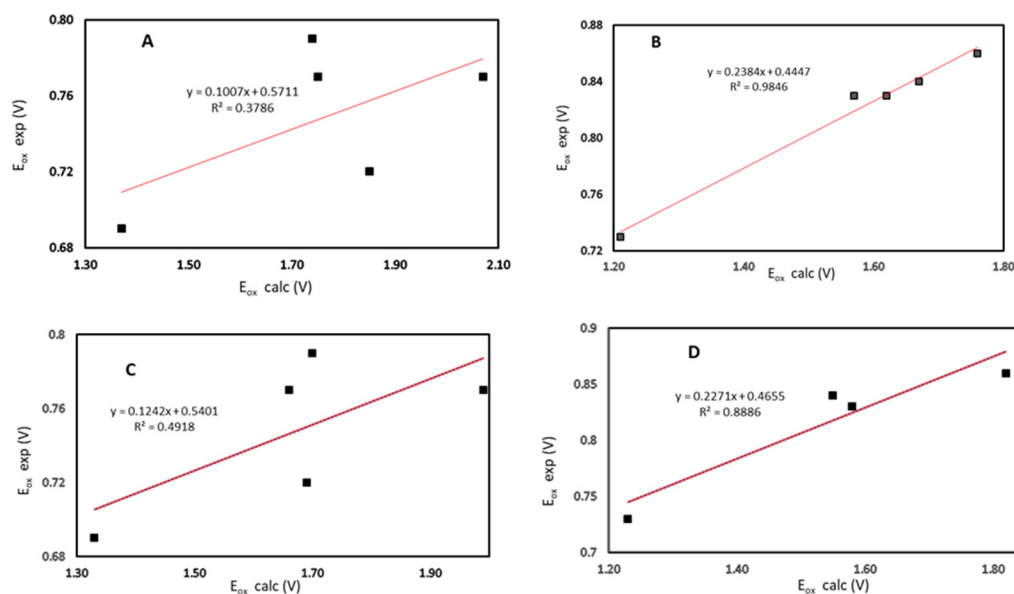


Figure 4. Experimental versus calculated oxidation potential for (A) compound **C1** to **C5** considering singlet oxidized species; (B) compound **C6** to **C10** considering singlet oxidized species; (C) compound **C1** to **C5** considering triplet oxidized species; (D) compound **C6** to **C10** considering triplet oxidized species.

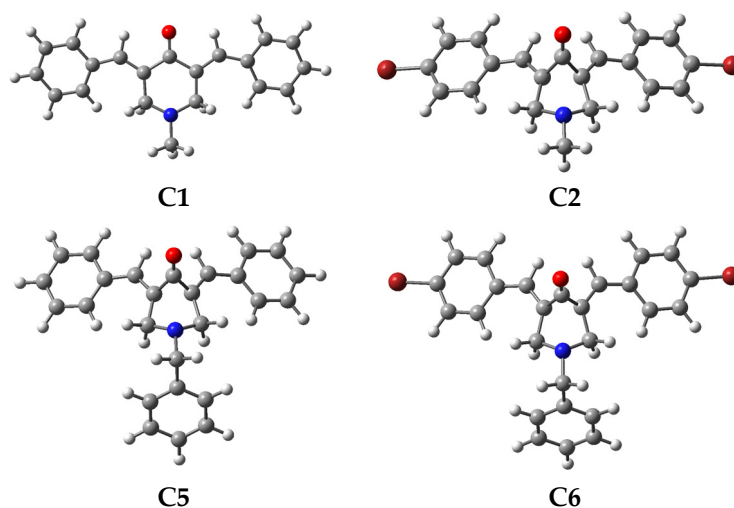


Figure 5. Optimized geometry at the M06/6-311+G(d,p) level for the oxidized species (singlet dication) of compound **C1**, **C2**, **C5**, and **C6**.

The geometry of the singlet and triplet oxidized species for all compounds are in Tables S1 and S2 of the Supplementary Materials.

To obtain insights into the behavior observed for these two series of compounds, we studied the energy of frontier molecular orbitals. In previous works, theoretical calculations of some of these compounds had been carried out to study their reactivity and the behavior of their radical anions [16], as well as optical properties [28]. In our previous work [16], we obtained, at the B3LYP/6-31G(d) level, the energies of the frontier molecular orbitals of some compounds studied here (**C1**, **C2**, **C3**, **C6**, **C7**, and **C8**). Table 7 shows the values

for HOMO and LUMO energies (E_{HOMO} and E_{LUMO} , respectively) and the HOMO–LUMO energy gap ($\text{GAP}_{\text{H-L}}$). These values, calculated at M06/6-311+G(d,p), showed slight differences from those calculated previously for some of the compounds at the B3LYP/6-31G(d) level. The E_{HOMO} values calculated at M06/6-311+G(d,p) tend to be lower, while the E_{LUMO} values tend to be higher, which leads to the $\text{GAP}_{\text{H-L}}$ being lower for M06/6-311+G(d,p). However, the tendency for the three compounds in common for each series is the same. Unsubstituted derivatives in the aromatic ring show the highest E_{HOMO} and E_{LUMO} , followed by *p*-Br and *p*-Cl (both for N-methyl and N-benzyl series). In addition, it can be observed that the value of $\text{GAP}_{\text{H-L}}$ did not show significant differences among compounds from the N-methyl and N-benzyl series.

Table 7. Calculated HOMO and LUMO energies, as well as the HOMO–LUMO gap energy ($\text{GAP}_{\text{H-L}}$). All values are in eV.

N-Substituent	Compound	E_{HOMO}	E_{LUMO}	$\text{GAP}_{\text{H-L}}$
N-methyl	C1	−6.6844	−2.3063	4.3781
	C2	−6.7519	−2.5410	4.2109
	C3	−6.7651	−2.5264	4.2387
	C4	−7.0932	−2.8377	4.2555
	C5	−6.1293	−2.0417	4.0875
N-benzyl	C6	−6.6296	−2.2766	4.3529
	C7	−6.7279	−2.5091	4.2188
	C8	−6.7392	−2.4940	4.2452
	C9	−7.0073	−2.8015	4.2058
	C10	−6.1144	−2.0193	4.0951

We examined the correlation among E_{HOMO} and experimental E_{ox} pairs, considering that electrons on this orbital are those that are removed in the oxidation process. Figure 6 shows the correlation for both the N-methyl and N-benzyl series. We found that the E_{HOMO} of N-benzyl derivatives correlates well with experimental E_{ox} , with an $R^2 = 0.9524$. On the other hand, N-methyl derivatives did not present a good correlation, obtaining an $R^2 = 0.6342$. These results also support the assumption that the oxidation of the N-methyl derivatives, unlike the N-benzyl ones, suffers a complex oxidation process that does not only involve the direct subtraction of two electrons from the HOMO.

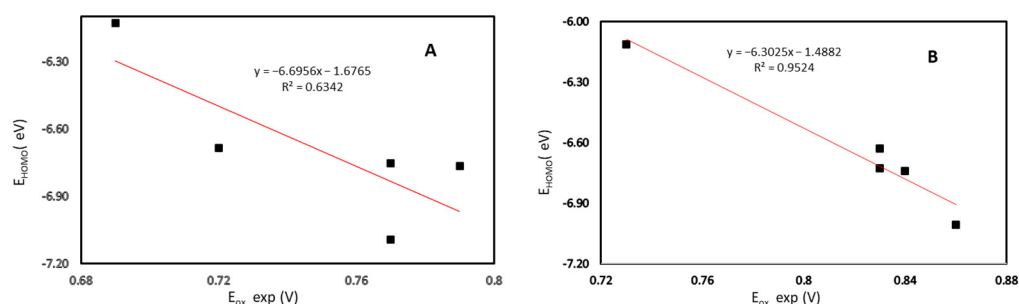


Figure 6. Experimental oxidation potential ($E_{\text{ox exp}}$) versus HOMO energy (E_{HOMO}) for (A) compounds C1 to C5, and (B) compounds C6 to C10.

To evaluate alternative possible mechanisms, which can imply the heterolytic cleavage of a carbon–hydrogen (C–H) bond, we study the bond dissociation enthalpies (BDEs) of the C–H bonds potentially breakable in compounds 1 and 6 (BDE1 and BDE2 in Table 8). A significant difference between the lower BDE would be indicative of a possible differential mechanism between the compounds of both series.

Table 8. Calculated C–H bond dissociation enthalpies (BDEs).

1. R = H
6. R = Ph

Compound	BDE1 [kcal/mol]	BDE2 [kcal/mol]
1	83.47	61.50
6	71.20	60.15

Results show that for both compounds, the BDE2 was the lowest, and there are no significant differences in the values (61.50 kcal/mol for **1** vs. 60.15 kcal/mol for **6**). The latter suggests that neither of the two series of compounds (N-methyl and N-benzyl derivatives) has a significant preference for the proton-coupled electron transfer (PCET) mechanism; therefore, this cannot explain the differences between both series.

A plausible explanation for the irreversible oxidation of the compounds is to consider a chemical reaction coupled to the electrochemical process. For heterocyclic tertiary amines, an electrochemical oxidation reaction (Shono oxidation) has been described that gives products with a substituent in the carbon vicinal to the nitrogen [30,40,41]. The process consists of a two-electron oxidation coupled to a proton transfer to generate an iminium cation intermediate which reacts with nucleophiles to achieve a great variety of products depending on the conditions [42–44]. In our case, it is possible that the attacking nucleophile corresponds to the same molecule generating a dimer. This hypothesis needs to be evaluated in future works that delve into mechanistic aspects of the oxidation of these compounds.

3. Materials and Methods

3.1. Synthesis

The synthesis of 4-piperidinone derivatives was performed in agreement with reported methods with slight modification (Table 1). To a solution of 1-methyl- or 1-benzyl-4-piperidone (0.30 g, 1.0 equivalent) in ethanol:water 1:1 (2 mL), KOH (0.3 g) was added and sonicated for 5 min. Then, the appropriate aldehyde (2.0 equivalents) was added, and the mixture was sonicated for 15 min at room temperature. The separated solid was filtered and washed with ethanol–water (20 mL) to obtain a yellow solid. Finally, product **C1** was crystallized from ethanol, compound **C5** was crystallized from methanol, and the other compounds were crystallized from a mixture of chloroform:methanol. Synthesis of the new compound (3E,5E)-1-benzyl-3,5-bis(4-(trifluoromethyl)benzylidene)piperidin-4-one (**C9**) was carried out as follows: to a solution of 1-benzyl 4-piperidone (0.30 g, 1.59 mmol) in ethanol:water 1:1 (2 mL), KOH (0.3 g) was added and sonicated for 5 min. Then, 4-trifluoromethylbenzaldehyde (0.55 g, 3.18 mmol) was added and the mixture was sonicated for 15 min at room temperature. The separated solid was filtered and washed with ethanol–water (20 mL) to obtain a yellow solid (0.83 g, 52% yield). Finally, the product was purified by column chromatography using hexane:ethyl acetate 4:1. ¹H RMN (400.13 MHz, CDCl₃) δ: 3.71 (s, 2H), 3.84 (s, 4H), 7.24 (s, 5H), 7.42 (d, *J* = 8.1 Hz, 4H), 7.63 (d, *J* = 8.1, 4H), 7.80 (s, 2H). ¹³C RMN (100.61 MHz, CDCl₃) δ: 54.1, 61.3, 123.9 (q, *J* = 271.8 Hz), 125.5 (q, *J* = 4.1), 127.6, 128.42, 128.9, 129.6, 130.2, 130.6 (q, *J* = 32.7), 134.9, 135.1, 136.9, 138.5, 187.27. M.p. 129.3–131.5 °C.

3.2. Electrochemical Experiments

Electrolytic medium: acetonitrile containing 0.1 M tetrabutylammonium perchlorate (TBAP) was used as the electrolytic medium and the working concentrations of each compound were 2 mM.

Differential pulse voltammetry (DPV), cyclic voltammetry (CV), square wave voltammetry, and electrochemical impedance spectroscopy (EIS) were carried out with a CH Instrument (CHI 750) electrochemical workstation. All electrochemical experiments were carried out with 2.0 mM of each piperidone derivative. A stationary glassy carbon electrode (GCE, CH Instrument with an area of 0.0707 cm²) was used as the working electrode. The surface of the electrode was polished to a mirror finish with 0.1 μm alumina powder before each experiment, and the surface was cleaned with ethanol under an ultrasonication for 30 s. A platinum spiral wire was used as an auxiliary electrode and the potentials were measured against a non-aqueous Ag/Ag⁺ reference electrode CH Instrument 112. All experiments were performed in ambient conditions.

3.3. Computational Details

All calculations were carried out using Gaussian 09 [45] program package, revision a.01; Gaussian, Inc.: Wallingford, CT, USA). Geometries were calculated without symmetry constraints at the DFT M06 and M06-2X level with the 6-311+G (d,p) basis set. The conductor-like polarizable continuum (C-PCM), which has shown good performance to redox potential calculations [8], was used to include the solvent effect (acetonitrile). No imaginary vibrational frequencies were found at the optimized geometries, indicating that they are the true minima of the potential energy surface.

In previous work [46], we applied a thermodynamic cycle to obtain the Gibbs free energy of the reaction in solution ($G^\circ(t)$) for calculation of the redox potentials of quinones, and we used the same approach here. Reduction potentials concerning the Ag/AgCl reference electrode were obtained by the following equation:

$$E_{red} = \frac{-\Delta G^\circ(t)}{nF} - 4.72 \text{ V} \quad (3)$$

where the value 4.72 V corresponds to the redox potential of the Ag/AgCl couple. Bond dissociation enthalpies were calculated following a previous methodology [8,47].

4. Conclusions

In this work, the electrochemical behavior of N-substituted-4-piperidone curcumin analogs was studied experimentally and theoretically. Oxidation potentials ranged from 0.72 to 0.89 V, with N-methyl-4-piperidones values approximately 0.1 V lower than those of N-benzyl-4-piperidones. We found that the electrochemical oxidation of these compounds implies a two-electron transfer process. Cyclic voltammetry studies showed that compounds suffer irreversible oxidation and suggested that it is a diffusion-controlled process. DFT quantum chemical calculations with M06 and M06-2x functionals showed that the former works better to calculate the oxidation potentials of these compounds. The results also suggested that the electronic state for oxidized species is a singlet. A good correlation between experimental and calculated oxidation potentials for N-benzyl-4-piperidones ($r = 0.9846$) showed that calculations were representative of the oxidation process. On the other hand, the calculated oxidation potentials for N-methyl-4-piperidones exhibited a poor correlation with the experimental values. The latter indicates that calculations do not represent the process well and suggests that the oxidation of N-methyl-4-piperidones is a more complex process. Calculations of the BDEs for labile C-H bonds in the compounds did not show significant differences, suggesting that neither of the two series of compounds has a significant preference for proton-coupled electron transfer (PCET). It was proposed that irreversible behavior of the compounds is due to a potential dimerization by a Shono-type oxidation reaction, which is a common electrochemical reaction in tertiary heterocyclic

amines. Future studies dealing with the potential mechanisms for the oxidation of these compounds need to be carried out to fully understand their electrochemical behavior.

Supplementary Materials: The following supporting information can be downloaded at: <https://www.mdpi.com/article/10.3390/ijms232315043/s1>, Table S1: Optimized geometries for triplet dications of all compounds at the DFT M06/6-311+G(d,p) level; Table S2. Optimized geometries for singlet dications of all compounds at the DFT M06/6-311+G(d,p) level; Optimized geometry cartesian coordinates of all compounds (neutral, singlet dication, and triplet dication).

Author Contributions: Conceptualization, R.A.-M. and M.M.-C. (Maximiliano Martínez-Cifuentes); Data curation, R.A.-M. and M.M.-C. (Maximiliano Martínez-Cifuentes); Formal analysis, M.M.-C. (Maximiliano Martínez-Cifuentes); Funding acquisition, R.A.-M. and M.M.-C. (Maximiliano Martínez-Cifuentes); Investigation, J.A., C.E.V., M.M.-C. (Matías Monroy-Cárdenas) and M.M.-C. (Maximiliano Martínez-Cifuentes); Methodology, J.A., R.A.-M. and M.M.-C. (Maximiliano Martínez-Cifuentes); Project administration, R.A.-M. and M.M.-C. (Maximiliano Martínez-Cifuentes); Software, M.M.-C. (Maximiliano Martínez-Cifuentes); Supervision, M.M.-C. (Maximiliano Martínez-Cifuentes); Validation, R.A.-M. and M.M.-C. (Maximiliano Martínez-Cifuentes); Visualization, J.A. and M.M.-C. (Maximiliano Martínez-Cifuentes); Writing—original draft, R.A.-M. and M.M.-C. (Maximiliano Martínez-Cifuentes); Writing—review & editing, R.A.-M. and M.M.-C. (Maximiliano Martínez-Cifuentes). All authors have read and agreed to the published version of the manuscript.

Funding: This research was funded by FONDECYT 1221874 (R.A.-M.), FONDECYT 11170142 (M.M.-C. (Maximiliano Martínez-Cifuentes)) and was supported by ACT210097-ANID. Powered@NLHPC: this research was partially supported by the supercomputing infrastructure of the NLHPC (ECM-02).

Institutional Review Board Statement: Not applicable.

Informed Consent Statement: Not applicable.

Data Availability Statement: Not applicable.

Conflicts of Interest: The authors declare no conflict of interest.

References

1. Agrawal, D.K.; Mishra, P.K. Curcumin and Its Analogues: Potential Anticancer Agents. *Med. Res. Rev.* **2010**, *30*, 818–860. [[CrossRef](#)] [[PubMed](#)]
2. Lin, J.Q.; Huo, X.; Liu, X.H. “mTOR Signaling Pathway”: A Potential Target of Curcumin in the Treatment of Spinal Cord Injury. *BioMed Res. Int.* **2017**, *2017*, 7. [[CrossRef](#)]
3. Yuan, J.Y.; Botchway, B.O.A.; Zhang, Y.; Tan, X.N.; Wang, X.Z.; Liu, X.H. Curcumin Can Improve Spinal Cord Injury by Inhibiting TGF- β -SOX9 Signaling Pathway. *Cell. Mol. Neurobiol.* **2019**, *39*, 569–575. [[CrossRef](#)] [[PubMed](#)]
4. Golonko, A.; Lewandowska, H.; Swislocka, R.; Jasinska, U.T.; Priebe, W.; Lewandowski, W. Curcumin as tyrosine kinase inhibitor in cancer treatment. *Eur. J. Med. Chem.* **2019**, *181*, 25. [[CrossRef](#)] [[PubMed](#)]
5. Zoi, V.; Galani, V.; Lianos, G.D.; Voulgaris, S.; Kyritsis, A.P.; Alexiou, G.A. The Role of Curcumin in Cancer Treatment. *Biomedicines* **2021**, *9*, 1086. [[CrossRef](#)] [[PubMed](#)]
6. Hasanzadeh, S.; Read, M.I.; Bland, A.R.; Majeed, M.; Jamialahmadi, T.; Sahebkar, A. Curcumin: An inflammasome silencer. *Pharmacol. Res.* **2020**, *159*, 15. [[CrossRef](#)] [[PubMed](#)]
7. Chainoglou, E.; Hadjipavlou-Litina, D. Curcumin in Health and Diseases: Alzheimer’s Disease and Curcumin Analogues, Derivatives, and Hybrids. *Int. J. Mol. Sci.* **2020**, *21*, 1975. [[CrossRef](#)] [[PubMed](#)]
8. Forero-Doria, O.; Guzman, L.; Jimenez-Aspee, F.; Echeverria, J.; Wehinger, S.; Valenzuela, C.; Araya-Maturana, R.; Martinez-Cifuentes, M. An In Vitro and In Silico Study of Antioxidant Properties of Curcuminoid N-alkylpyridinium Salts: Initial Assessment of Their Antitumoral Properties. *Antioxidants* **2022**, *11*, 1104. [[CrossRef](#)]
9. Martínez-Cifuentes, M.; Monroy-Cardenas, M.; Millas-Vargas, J.P.; Weiss-Lopez, B.E.; Araya-Maturana, R. Assessing Parameter Suitability for the Strength Evaluation of Intramolecular Resonance Assisted Hydrogen Bonding in o-Carbonyl Hydroquinones. *Molecules* **2019**, *24*, 280. [[CrossRef](#)]
10. Nelson, K.M.; Dahlin, J.L.; Bisson, J.; Graham, J.; Pauli, G.F.; Walters, M.A. The Essential Medicinal Chemistry of Curcumin. *J. Med. Chem.* **2017**, *60*, 1620–1637. [[CrossRef](#)]
11. Bairwa, K.; Grover, J.; Kania, M.; Jachak, S.M. Recent developments in chemistry and biology of curcumin analogues. *RSC Adv.* **2014**, *4*, 13946–13978. [[CrossRef](#)]
12. Martínez-Cifuentes, M.; Weiss-Lopez, B.; Santos, L.S.; Araya-Maturana, R. Heterocyclic Curcumin Derivatives of Pharmacological Interest: Recent Progress. *Curr. Top. Med. Chem.* **2015**, *15*, 1663–1672. [[CrossRef](#)] [[PubMed](#)]

13. Zhao, S.J.; Pi, C.; Ye, Y.; Zhao, L.; Wei, Y.M. Recent advances of analogues of curcumin for treatment of cancer. *Eur. J. Med. Chem.* **2019**, *180*, 524–535. [[CrossRef](#)] [[PubMed](#)]
14. Liang, G.A.; Shao, L.L.; Wang, Y.; Zhao, C.G.; Chu, Y.H.; Xiao, J.; Zhao, Y.; Li, X.K.; Yang, S.L. Exploration and synthesis of curcumin analogues with improved structural stability both in vitro and in vivo as cytotoxic agents. *Bioorg. Med. Chem.* **2009**, *17*, 2623–2631. [[CrossRef](#)]
15. Schneider, C.; Gordon, O.N.; Edwards, R.L.; Luis, P.B. Degradation of Curcumin: From Mechanism to Biological Implications. *J. Agric. Food Chem.* **2015**, *63*, 7606–7614. [[CrossRef](#)]
16. Martinez-Cifuentes, M.; Weiss-Lopez, B.; Araya-Maturana, R. A Computational Study of Structure and Reactivity of N-Substituted-4-Piperidones Curcumin Analogues and Their Radical Anions. *Molecules* **2016**, *21*, 1658. [[CrossRef](#)]
17. Bazzaro, M.; Anchoori, R.K.; Mudiam, M.K.R.; Issaenko, O.; Kumar, S.; Karanam, B.; Lin, Z.H.; Vogel, R.I.; Gavioli, R.; Destro, F.; et al. Alpha,beta-Unsaturated Carbonyl System of Chalcone-Based Derivatives Is Responsible for Broad Inhibition of Proteasomal Activity and Preferential Killing of Human Papilloma Virus (HPV) Positive Cervical Cancer Cells. *J. Med. Chem.* **2011**, *54*, 449–456. [[CrossRef](#)]
18. Nunes, L.M.; Hossain, M.; Varela-Ramirez, A.; Das, U.; Ayala-Marin, Y.M.; Dimmock, J.R.; Aguilera, R.J. A novel class of piperidones exhibit potent, selective and pro-apoptotic anti-leukemia properties. *Oncol. Lett.* **2016**, *11*, 3842–3848. [[CrossRef](#)]
19. Nouredin, S.A.; El-Shishtawy, R.M.; Al-Footy, K.O. Curcumin analogues and their hybrid molecules as multifunctional drugs. *Eur. J. Med. Chem.* **2019**, *182*, 40. [[CrossRef](#)]
20. Razali, N.S.C.; Lam, K.W.; Rajab, N.F.; Jamal, A.R.A.; Kamaluddin, N.F.; Chan, K.M. Curcumin piperidone derivatives induce anti-proliferative and anti-migratory effects in LN-18 human glioblastoma cells. *Sci. Rep.* **2022**, *12*, 17. [[CrossRef](#)]
21. Kostrzewa, T.; Wolosewicz, K.; Jamrozik, M.; Drzewdzon, J.; Sieminska, J.; Jacewicz, D.; Gorska-Ponikowska, M.; Kolaczkowski, M.; Lazny, R.; Kuban-Jankowska, A. Curcumin and Its New Derivatives: Correlation between Cytotoxicity against Breast Cancer Cell Lines, Degradation of PTP1B Phosphatase and ROS Generation. *Int. J. Mol. Sci.* **2021**, *22*, 10368. [[CrossRef](#)] [[PubMed](#)]
22. Gorman, A.A.; Hamblett, I.; Srinivasan, V.S.; Wood, P.D. Curcumin-derived transients—A pulsed-laser and pulse-radiolysis study. *Photochem. Photobiol.* **1994**, *59*, 389–398. [[CrossRef](#)] [[PubMed](#)]
23. Jovanovic, S.V.; Steenken, S.; Boone, C.W.; Simic, M.G. H-atom transfer is a preferred antioxidant mechanism of curcumin. *J. Am. Chem. Soc.* **1999**, *121*, 9677–9681. [[CrossRef](#)]
24. Priyadarsini, K.I.; Maity, D.K.; Naik, G.H.; Kumar, M.S.; Unnikrishnan, M.K.; Satav, J.G.; Mohan, H. Role of phenolic O-H and methylene hydrogen on the free radical reactions and antioxidant activity of curcumin. *Free Radic. Biol. Med.* **2003**, *35*, 475–484. [[CrossRef](#)] [[PubMed](#)]
25. Litwinienko, G.; Ingold, K.U. Solvent effects on the rates and mechanisms of reaction of phenols with free radicals. *Acc. Chem. Res.* **2007**, *40*, 222–230. [[CrossRef](#)]
26. Jha, N.S.; Mishra, S.; Jha, S.K.; Suroliya, A. Antioxidant activity and electrochemical elucidation of the enigmatic redox behavior of curcumin and its structurally modified analogues. *Electrochim. Acta* **2015**, *151*, 574–583. [[CrossRef](#)]
27. Belmont-Bernal, F.; Aguilar, J.C.; Ramos, E.; Guadarrama, P. Systematic Derivatization of Curcumin and its Effect on Antioxidant Capacity and Action Mechanism. Cyclic Voltammetry and DFT as Tools of Analysis. *Chemistryselect* **2016**, *1*, 5091–5098. [[CrossRef](#)]
28. Saeed, B.A.; Hassan, Q.M.A.; Emshary, C.A.; Sultan, H.A.; Elias, R.S. The nonlinear optical properties of two dihydropyridones derived from curcumin. *Spectrochim. Acta Part A-Mol. Biomol. Spectrosc.* **2020**, *240*, 14. [[CrossRef](#)]
29. Atkins, A.P.; Rowett, A.C.; Heard, D.M.; Tate, J.A.; Lennox, A.J.J. Electrochemical Benzylic C(sp³)-H Acyloxylation. *Org. Lett.* **2022**, *24*, 5105–5108. [[CrossRef](#)]
30. Wang, F.; Stahl, S.S. Electrochemical Oxidation of Organic Molecules at Lower Overpotential: Accessing Broader Functional Group Compatibility with Electron-Proton Transfer Mediators. *Acc. Chem. Res.* **2020**, *53*, 561–574. [[CrossRef](#)]
31. Tereshchenko, O.D.; Perebiynis, M.Y.; Knysh, I.V.; Vasylets, O.V.; Sorochenko, A.A.; Slobodyanyuk, E.Y.; Rusanov, E.B.; Borysov, O.V.; Kolotilov, S.V.; Ryabukhin, S.V.; et al. Electrochemical Scaled-up Synthesis of Cyclic Enecarbamates as Starting Materials for Medicinal Chemistry Relevant Building Blocks. *Adv. Synth. Catal.* **2020**, *362*, 3229–3242. [[CrossRef](#)]
32. Laviron, E. General expression of the linear potential sweep voltammogram in the case of diffusionless electrochemical systems. *J. Electroanal. Chem.* **1979**, *101*, 19–28. [[CrossRef](#)]
33. Paukku, Y.; Hill, G. Theoretical Determination of One-Electron Redox Potentials for DNA Bases, Base Pairs, and Stacks. *J. Phys. Chem. A* **2011**, *115*, 4804–4810. [[CrossRef](#)] [[PubMed](#)]
34. Zhang, W.N.; Yang, T.; Zhao, K.; Liao, X.B.; Zhao, Y. Accurate redox potentials for solvents in Li-metal batteries and assessment of density functionals. *Int. J. Quantum Chem.* **2022**, *122*, 11. [[CrossRef](#)]
35. Lewis, K.; Copeland, K.; Hill, G. One-Electron Redox Properties of DNA Nucleobases and Common Tautomers. *Int. J. Quantum Chem.* **2014**, *114*, 1678–1684. [[CrossRef](#)]
36. Pittman, K.M.; McAlexander, H.R.; Tschumper, G.S.; Shukla, M.K. Computational Investigation on Electronic Structures and Properties of 4,6-Bis(nitroimino)-1,3,5-triazinan-2-one: An Insensitive Munition Compound. *J. Phys. Chem. A* **2019**, *123*, 3504–3509. [[CrossRef](#)]
37. Isegawa, M.; Neese, F.; Pantazis, D.A. Ionization Energies and Aqueous Redox Potentials of Organic Molecules: Comparison of DFT, Correlated ab Initio Theory and Pair Natural Orbital Approaches. *J. Chem. Theory Comput.* **2016**, *12*, 2272–2284. [[CrossRef](#)]
38. Wang, D.; Huang, S.P.; Wang, C.; Yue, Y.; Zhang, Q.S. Computational prediction for oxidation and reduction potentials of organic molecules used in organic light-emitting diodes. *Org. Electron.* **2019**, *64*, 216–222. [[CrossRef](#)]

39. Lucia-Tamudo, J.; Cardenas, G.; Anguita-Ortiz, N.; Diaz-Tendero, S.; Nogueira, J.J. Computation of Oxidation Potentials of Solvated Nucleobases by Static and Dynamic Multilayer Approaches. *J. Chem. Inf. Modeling* **2022**, *62*, 3365–3380. [[CrossRef](#)]
40. Shono, T.; Matsumura, Y.; Tsubata, K. Electroorganic chemistry.46. A new carbon-carbon bond forming reaction at the alpha-position of amines utilizing anodic-oxidation as a key step. *J. Am. Chem. Soc.* **1981**, *103*, 1172–1176. [[CrossRef](#)]
41. Yamamoto, K.; Kuriyama, M.; Onomura, O. Shono-type Oxidation for Functionalization of N-Heterocycles. *Chem. Rec.* **2021**, *21*, 2239–2253. [[CrossRef](#)] [[PubMed](#)]
42. Gunasekera, D.; Mahajan, J.P.; Wanzi, Y.; Rodrigo, S.; Liu, W.; Tan, T.; Luo, L. Controlling One- or Two-Electron Oxidation for Selective Amine Functionalization by Alternating Current Frequency. *J. Am. Chem. Soc.* **2022**, *144*, 9874–9882. [[CrossRef](#)] [[PubMed](#)]
43. Vu, V.H.; Louafi, F.; Girard, N.; Marion, R.; Roisnel, T.; Dorcet, V.; Hurvois, J.P. Electrochemical Access to 8-(1-Phenyl-ethyl)-1,4-dioxo-8-aza-spiro 4.5 decane-7-carbonitrile. Application to the Asymmetric Syntheses of (+)-Myrtine and Alkaloid (+)-241D. *J. Org. Chem.* **2014**, *79*, 3358–3373. [[CrossRef](#)] [[PubMed](#)]
44. Gao, P.S.; Weng, X.J.; Wang, Z.H.; Zheng, C.; Sun, B.; Chen, Z.H.; You, S.L.; Mei, T.S. Cu-II/TEMPO-Catalyzed Enantioselective C(sp³)-H Alkynylation of Tertiary Cyclic Amines through Shono-Type Oxidation. *Angew. Chem. Int. Ed.* **2020**, *59*, 15254–15259. [[CrossRef](#)]
45. Frisch, M.J.; Trucks, G.W.; Schlegel, H.B.; Scuseria, G.E.; Robb, M.A.; Cheeseman, J.R.; Scalmani, G.; Barone, V.; Mennucci, B.; Petersson, G.; et al. *Gaussian 09*; Gaussian, Inc.: Wallingford, CT, USA, 2009.
46. Martinez-Cifuentes, M.; Salazar, R.; Ramirez-Rodriguez, O.; Weiss-Lopez, B.; Araya-Maturana, R. Experimental and Theoretical Reduction Potentials of Some Biologically Active ortho-Carbonyl para-Quinones. *Molecules* **2017**, *22*, 577. [[CrossRef](#)] [[PubMed](#)]
47. Galano, A.; Alvarez-Idaboy, J.R. Computational strategies for predicting free radical scavengers' protection against oxidative stress: Where are we and what might follow? *Int. J. Quantum Chem.* **2019**, *119*, 23. [[CrossRef](#)]